ACS OMEGA

Article

Cite This: ACS Omega 2018, 3, 13413−13421

http://pubs.acs.org/journal/acsodf

Piezoelectric Response of Porous Nanotubes Derived from Hexagonal Boron Nitride under Strain Influence

Guilherme S. L. Fabris,[†] Naiara L. Marana,[†] Elson Longo,[‡] and Julio R. Sambrano*,[†]

[†]Modeling and Molecular Simulation Group—CDMF, São Paulo State University, Bauru 17033-360, São Paulo, Brazil

[‡]Chemistry Institute—CDMF, Federal University of São Carlos, P.O. Box 14801-907, São Carlos 13565-905, São Paulo, Brazil

Supporting Information

ABSTRACT: A computational study via periodic density functional theory of porous nanotubes derived from single-layer surfaces of porous hexagonal boron nitride nanotubes (PBNNTs) and inorganic graphenylene-like boron nitride nanotubes (IGP-BNNTs) has been carried out with the main focus in its piezoelectric behavior. The simulations showed that the strain provides a meaningful improve in the piezoelectric response on the zigzag porous boron nitride nanotubes. Additionally, its stability, possible formation, elastic, and electronic properties were analyzed, and for comparison purpose, the porous graphene and graphenylene nanotubes were studied. From the elastic properties study, it was found that IGP-BNNTs exhibited a higher rigidity because of the influence of the superficial porous area, as compared to PBNNTs. The present study provides evidence that the strain is a way to maximize the piezoelectric response and make this material a good candidate for electromechanical devices.

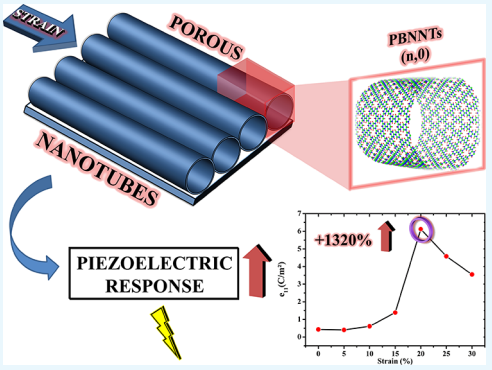

1. INTRODUCTION

Because of the discovery of graphene,[1] the interest in carbon-based structures with honeycomb networks has considerably increased because of their potential applications in nanodevices,[1,2] supercapacitors,[3] theranostics,[4] immunotherapy,[5] and fuel cells.[6] However, the zero band gap of graphene can limit its application in specific electronic devices; thus, there has been considerable activity in the development of techniques to overcome this limitation. Modifications to the structural, electronic, and chemical properties of graphene using different chemical[7−10] and physical[11−13] methods, or application of an electromagnetic field,[14] have been utilized to open and find a band gap suitable for electronic device applications.

Other alternative to surpass the current limitations of graphene structures is the inorganic graphene analogues, such as silicene,[15,16] germanene,[17] and hexagonal boron nitride (hBN),[18] because of their interesting properties. In addition, an ordered pore formation can be used as an alternative to modify their properties and confer various desirable characteristics, for example, as seen in recent graphene derivatives such as porous graphene (PG)[19−23] and graphenylene (GP),[23−26] which, unlike graphene, have semiconducting behavior. Recently, Yu and co-workers showed that GP has a great potential as an anode material for lithium batteries with high-storage capabilities[27] as well as a molecular sieve for gas.[28]

On the other hand, hBN is of particular interest as it has the same honeycomb topology and similar bond lengths and lattice parameters (with a mismatch of ∼1.8%) as graphene[29] but has different electronic properties with a wide band gap of ∼5.96 eV.[30]

In a recent paper, it was presented that the inorganic counterparts for PG and GP surfaces, namely porous boron nitride (PBN) and inorganic GP-like boron nitride (IGP-BN) structures,[23] both of which have a similar band gap to hBN. However, unlike GP, IGP-BN is not suitable for direct use as an anode material but requires prior doping with carbon atoms, as shown by Hankel and Searles.[31]

The idea of rolling up a single-layer surface to construct nanotubes opens numerous possibilities for the applications, from energy harvesting and storage to molecular sieves.[32] Furthermore, the production of nanotubes has been extended to inorganic materials such as zinc oxide,[33] titanium dioxide,[34] aluminum nitride,[35] boron nitride,[36] and other systems. These inorganic nanotubes can have advantages over CNTs in certain applications, such as electronics, because of their unique properties.[37,38]

In 2015, Koch et al.[39] proposed GP nanotubes (GPNTs) and used plane-wave density functional theory (DFT) combined with a Perdew−Burke−Ernzerhof (PBE) functional [in comparison with the density functional tight binding (DFTB)] to calculate metallic characteristics for armchair nanotubes with small diameters and small band gap semiconducting characteristics for nanotubes with larger diameters; they also show that GPNTs also have a promising lithium

Received: July 12, 2018
Accepted: October 2, 2018
Published: October 17, 2018

DOI: 10.1021/acsomega.8b01634
ACS Omega 2018, 3, 13413−13421

storage application because it retains their mechanical properties during charging cycles.

Fabris et al.[40] studied PG nanotubes (PGNTs) and GPNTs for nanotubes with diameters less than 56 Å using the DFTB method, which showed that PGNTs have a wide band gap of ∼3.3 eV, whereas GPNTs have a small band gap of ∼0.7 eV. They also showed that as the diameter of the PGNTs increases, the band gap decreases, whereas for GPNTs, the band gap increases with the PGNT diameter; these results are in agreement with those presented by Koch.

Although there have been several studies on carbon-based porous nanotubes, as described above, more detailed studies on the properties of these structures are required, such as on the elastic, piezoelectric, and vibrational properties.

Therefore, the present study proposes, for the first time, an inorganic counterpart for PGNTs and GPNTs, namely PBN nanotubes (PBNNTs) and IGP-BN nanotubes (IGP-BNNTs). Here, the structural, electronic, elastic properties, and the possible piezoelectricity activity of the armchair and zigzag conformations of PBNNTs and IGP-BNNTs using a periodic DFT methodology combined with a modified hybrid B3LYP functional and a triple-zeta plus polarization (TZVP) all-electron basis set were investigated.[41] Additionally and for comparison purpose were studied, at the same computational level, the properties of PGNTs and GPNTs.

These theoretical findings may provide an important information for experimental research, opening a rational development to the designing of alternative nanoelectronic devices.

2. MODELED SYSTEMS

PBN and IGP-BN are described by the $P\bar{6}m2$ and P_6/m space group, respectively, where PBN has a direct wide band gap of 6.45 eV with one lattice parameter ($a = b = 7.662$ Å), and IGP-BN has an indirect wide band gap of 5.52 eV with one lattice parameter ($a = b = 6.818$ Å).[23]

The PG surface has an indirect wide band gap of 3.78 eV and belongs to the space group $C222$ with two lattice parameters ($a = 7.426$ Å and $b = 7.437$ Å). GP has a direct band gap of 0.83 eV and belongs to the $P6/mmm$ symmetry group with one lattice parameter ($a = b = 6.735$ Å).[23]

PG and PBN models, Figure 1, can be achieved by replacing each atom of the graphene or hBN unit cell by a benzene-like ring with three hydrogen atoms alternating between two nonconsecutive atoms. Alternatively, GP and IGP-BN can be obtained by replacing each atom of the unit cell with a dimer of benzene-like rings joined by a square ring.

The first step for the construction of porous nanotubes involved the total energy optimization of lattice parameters and internal coordinates of the PBN, IGP-BN, PG, and GP porous surfaces. The second step was to construct porous nanotubes from the optimized porous surfaces (see Figure 1).

Two rolling directions of the surfaces are selected, zigzag ($\theta = 0°$) and armchair ($\theta = 30°$), represented by the indices (n, 0) and (n, n), respectively, where n is an integer that determines the diameter and chirality of the nanotube (Figure 1). Armchair and zigzag porous nanotubes with n = 2, 3, ..., 10, 15, 20, 23, 25, 27, and 30 were selected. In total, 15 armchair and zigzag nanotubes were constructed for each of the four porous structures, resulting in a total of 120 nanotube models.

The equations describing the number of atoms (n_T) for porous nanotubes can be easily obtained from the equations for nonporous nanotubes.[42] For PGNTs and PBNNTs, $n_T = 36\cdot(n^2 + nm + m^2)/d_R$, and for GPNTs and IGP-BNNTs, $n_T = 24\cdot(n^2 + nm + m^2)/d_R$, where d_R is the maximum common divisor of $(2n + m, 2m + n)$.

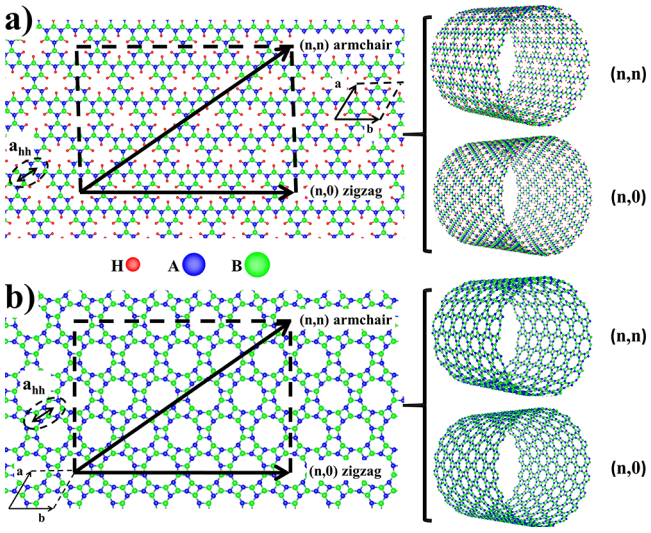

Figure 1. Generic scheme for porous nanotube construction: (a) from PBN surface forming PBNNTs with armchair (n, n) and zigzag (n, 0) symmetries; (b) from porous inorganic GP surface forming inorganic GPNTs with armchair (n, n) and zigzag (n, 0) symmetries.

The diameter, D, of porous nanotubes can be described in an analogous form to a perfect carbon nanotube as a function of n and m and is defined by $D = a_{hh}\cdot\sqrt{3(n^2 + nm + m^2)}/d_R$, where a_{hh} is the distance between two consecutive hexagons (in a typical carbon nanotube, this would be the C−C bond length), as can be seen in Figure 1. Thus, the smallest and biggest nanotube has 48 atoms with ∼4 Å of diameter, and the largest nanotube has 1080 atoms with ∼126 Å of diameter, respectively.

3. RESULTS AND DISCUSSION

3.1. Structural Properties. To better understand the stability and formation of these nanotubes, the energy necessary to roll up a nanotube from the surface, known as strain energy, $E_{strain} = (E_{NT}/n_{NT}) - E_{surface}$, where $E_{surface}$ is the total surface energy, E_{NT} is the total energy of the nanotube, and n_{NT} is the number of atoms on the unit cell, was calculated.

Analysis of the E_{strain} can help to predict the nanotube conformation (armchair or zigzag) which is probably formed and thus the most probable one to be obtained experimentally. Figure 2 depicts the relationship between E_{strain} and the porous nanotube diameter.

The number of atoms (n_T), the optimized nanotube diameter (D) and length (L), band gap energy (E_{gap}), and strain energy (E_{strain}) for PGNTs, GPNTs, PBNNTs, and IGP-BNNTs are displayed in Tables S1 and S2, respectively (see Supporting Information).

In general, an increase in the diameter implies a decrease in the strain energy. As shown in Figure 2, there are a convergence in the (7, 7) and (10, 0) nanotubes, indicating a convergence on diameter of ∼20 Å. PBNNTs, IGP-BNNTs, and GPNTs exhibited a smooth decrease in the strain energy but PGNTs had a small oscillation around −0.01 eV/atom. These results indicated that larger diameter nanotubes are more probable to be formed than smaller diameter nanotubes, regardless of the conformation (armchair or zigzag); also from

DOI: 10.1021/acsomega.8b01634
ACS Omega 2018, 3, 13413−13421

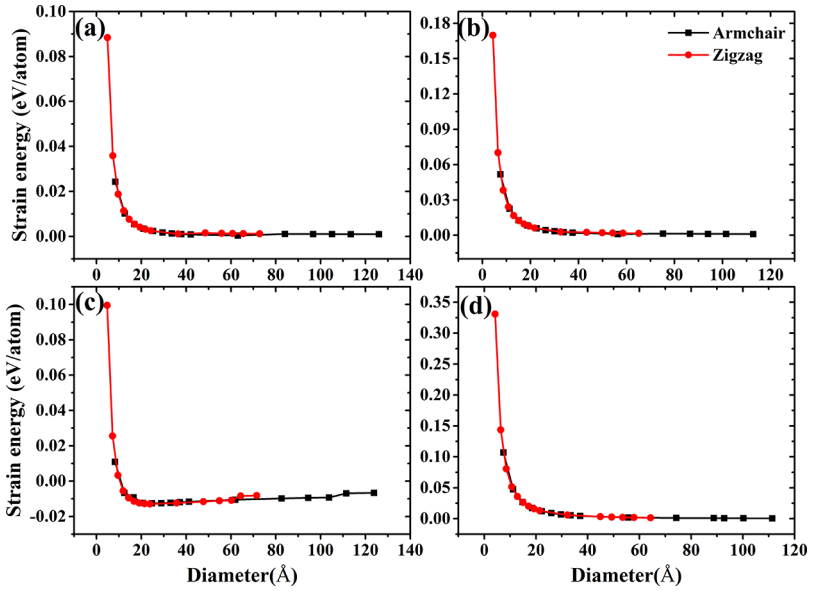

Figure 2. Strain energy (eV/atom) as a function of the diameter (Å) for: (a) PBNNTs, (b) IGP-BNNTs, (c) PGNTs, and (d) GPNTs.

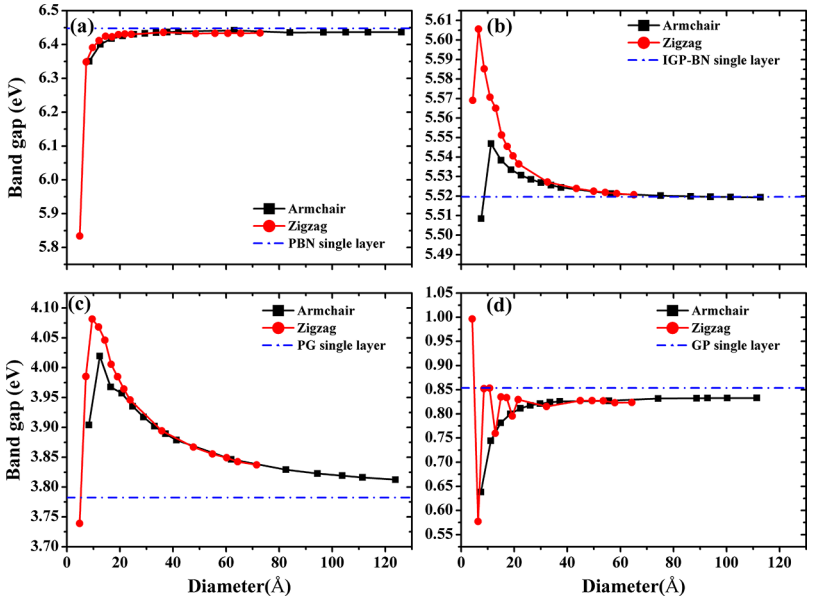

Figure 3. Band gap energy (eV) as a function of the diameter (Å) for (a) PBNNTs, (b) IGP-BNNTs, (c) PGNTs, and (d) GPNTs.

an experimental point of view, a highly controllable synthesis method is required to obtain small-diameter nanotubes.

Figure S1 illustrates porous nanotubes, highlighting the intra-ring and inter-ring bond lengths with additional comment about the nanotube geometry.

Therefore, even the nanotubes with the smallest diameter, such as (2, 2) and (2, 0) nanotubes, showed similar geometries as their respective surfaces, which were different from what were expected because the surfaces of nanotubes with small diameters tend to have a greater degree of geometry distortion.

It is important to note that despite maintaining the bond length and bond angles of single layers, rolling up of the nanotube single layers lead to a small distortion in the pore diameter, particularly for the smallest nanotubes. For armchair and zigzag PGNTs, the pore diameters were 3.87 and 3.79 Å, respectively, and for GPNTs, PBNNTs, and IGP-BNNTs, the pore diameters were 5.47, 3.79, and 5.59 Å for both armchair and zigzag chiralities, respectively. Compared with our previous work regarding porous surfaces,[23] the PGNTs, PBNNTs, and IGP-BNNTs exhibited a small increase in the pore diameter (3.6, 3.3, and 1.4%, respectively), whereas the GPNTs had the same diameter. This modification to the pore diameter could allow some molecules to pass through them, enabling them to act as a nanofilter for big molecules in which they can be stored inside the nanotube.

According to the QTAIMAC analysis (summarized in Table 2 and Figures 6, S4, and S5), the general description of the B−N bond belongs to the transit region, neither ionic nor covalent. However, the bond critical points (BCPs) for both PBNNT and IGP-BNNT are located closer to the boron atoms, ∼0.49 Å, indicating that the bond is located mostly around one nuclear attractor. Besides that, the positive values of the Laplacian and BCP densities around 0.18 e/bohr^3 suggest an ionic nature of the B−N bonds. On the other

DOI: 10.1021/acsomega.8b01634
ACS Omega 2018, 3, 13413−13421

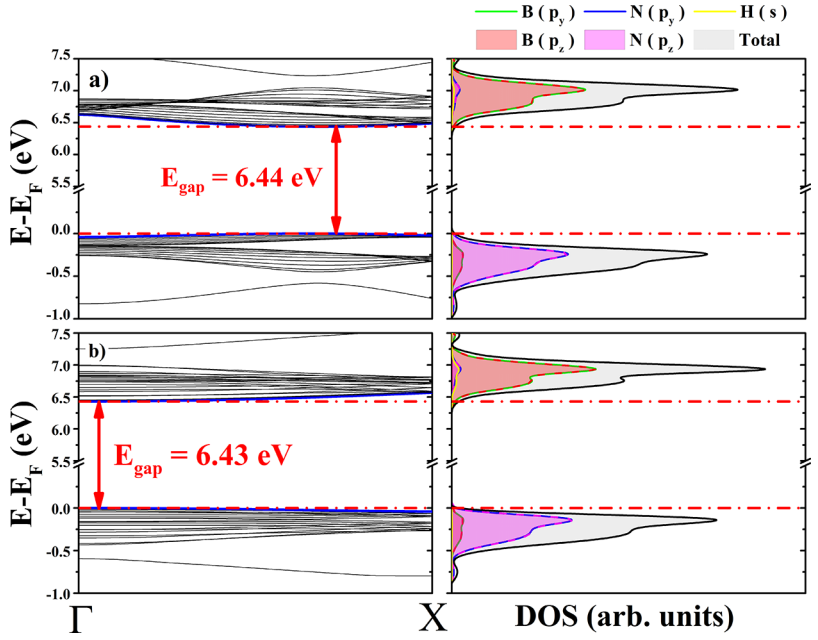

Figure 4. Band structure and DOS of (a) (10, 10) PBNNT and (b) (10, 0) PBNNT.

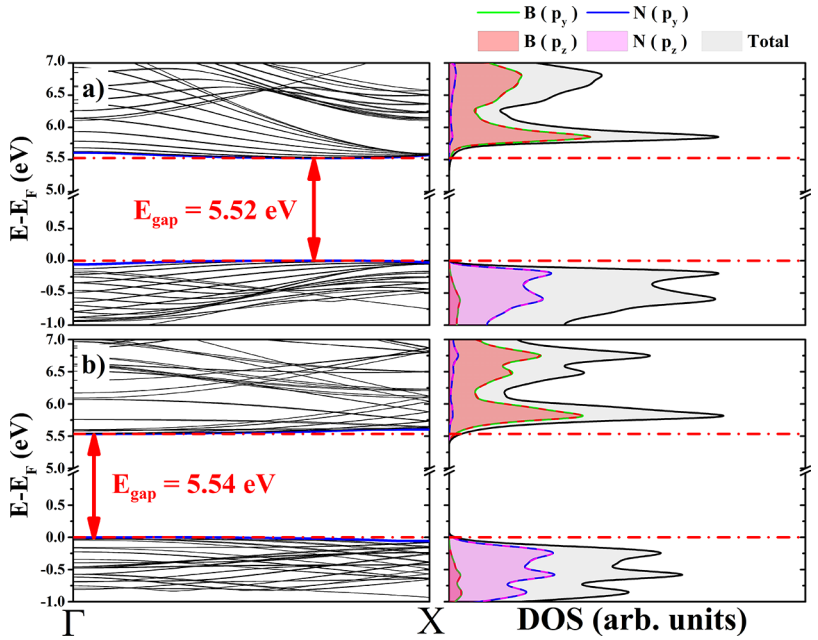

Figure 5. Band structure and DOS of (a) (10, 10) IGP-BNNT and (b) (10, 0) IGP-BNNT.

hand, the very small value of ellipticity, ε, highlights the cylindrically symmetric shape of the bonds and confirms the directionality of the bond. In this sense, because the bond has characteristics of both bond descriptions, it is considered a transitory type. The transitory bond character was also observed for porous sheets in previous work,[23] and although there was a great structural distortion when rolling the surface in nanotube, there was no modification in the type of bond of these systems.

3.2. Electronic Properties. Analysis of the band gap and porous nanotube trends, as shown in Figure 3, revealed a smooth increase in the band gap energy of the PBNNTs (Figure 3a) with the diameter and converged to the band gap of a single-layer PBN (~6.45 eV); however, IGP-BNNTs (Figure 3b) exhibited a decrease in their band gap as the diameter increased and converged to ~5.49 eV, which was also close to the band gap of their pristine surface (~5.54 eV). Compared with the BNNTs (~6.03 eV), the PBNNTs have an increase of ~7% and the IGP-BNNTs have a decrease of ~8% in the band gap, and the bands of both porous nanotubes are slightly flatter than the BNNTs. For PGNTs (Figure 3c), the band gap energy increases up to ~10 Å, after which the band gap gradually decreased and approached the band gap (~3.78 eV) of the single-layer PG. GPNTs (Figure 3d) exhibited a small band gap oscillation as the diameter increased, converging to a band gap of ~0.82 eV, which is close to that of their pristine surface (~0.85 eV). This effect can be associated to a higher nanotube structural tension of the

DOI: 10.1021/acsomega.8b01634
ACS Omega 2018, 3, 13413−13421

smaller diameter nanotubes, together with the oscillation of the $2p_y$ and $2p_z$ orbital contribution.

In comparison with the DFT/PBE results of Koch et al.,[39] the calculated band gap energy of GPNTs was quite different. Koch showed that for a particular chirality, GPNTs have a metallic behavior similar to that for CNTs.[43] The difference in results was due to the well-known fact that the PBE functional underestimates the band gap energy; however, considering whether the band gap is direct or indirect, our results were coincident for both chiralities. Also, when compared with a previous theoretical study[40] that utilized the DFTB methodology, the band gap behaviors for PGNTs and GPNTs were also in agreement, and the trend observed in the diameter dependence of the band gap was in reasonable agreement with this work.

To illustrate the electronic properties, two representative porous nanotubes, (10, 10) and (10, 0), with diameters of approximately 20 Å were chosen, because of their stabilization of the strain energy.

Figures 4 and 5 show representative band structures and density of states (DOS) for armchair (10, 10) and zigzag (10, 0) PBNNTs and IGP-BNNTs; the PGNTs and GPNTs can be seen in Figures S2 and S3 (see Supporting Information).

The (10, 10) and (10, 0) PBNNTs (Figure 4a,b) had band gap energies of 6.44 and 6.43 eV, respectively, both directing at the Γ point. The (10, 10) and (10, 0) IGP-BNNTs (Figure 5a,b) had band gaps of 5.53 eV (indirect between the Γ and ∼X points) and 5.54 eV (direct at the Γ point), respectively. As a reference, single-layer PBN and IGP-BN had band gap energies of 6.45 eV (direct at the K point) and 5.52 eV (indirect between the $M-K$ and K points), respectively.

The DOS of the armchair and zigzag PBNNTs (Figure 4a,b) showed that the main contribution to the valence band (VB) was from the $2p_y$ and $2p_z$ orbitals of the nitrogen atoms, with an additional small contribution from the $2p_y$ and $2p_z$ orbitals of the boron atoms. The conduction band (CB) displayed the reverse behavior, with the main contribution close to the band gap region arising from the $2p_y$ and $2p_z$ orbitals of the boron atoms, with a minor contribution from the $2p_y$ and $2p_z$ orbitals of the nitrogen atoms. There was also a small contribution from the 1s orbitals of the hydrogen atoms to the conduction and VBs.

For the armchair and zigzag IGP-BNNTs (Figure 5a,b), the main contributions to the valence and CBs were from the $2p_y$ and $2p_z$ orbitals of the nitrogen and boron atoms, respectively. The $2p_x$ orbitals did not contribute around the band gap of PBNNTs and IGP-BNNTs.

The (10, 10) and (10, 0) PGNTs (Figure S2a,b) had band gap energies of 3.88 eV (indirect between the Γ and ∼X points) and 3.95 eV (direct at the Γ point), respectively. These values were close to the calculated indirect band gap (3.78 eV) for the PG single-layer surface.

The (10, 10) and (10, 0) GPNTs (Figure S3a,b) had approximately the same band gap energy of 0.83 eV (both direct at the Γ point), respectively. The calculated nanotube band gap was very close to that of the GP single-layer surface (direct band gap energy of 0.83 eV).

Analysis of the DOS of armchair and zigzag PGNTs (Figure S2a,b) revealed that the main contribution to the top of the VB and bottom of the CB arises from the $2p_y$ and $2p_z$ orbitals of the carbon atoms, with a small contribution from the 1s orbital of the hydrogen atoms. Similarly, the valence and CBs of armchair and zigzag GPNTs (according to Figure S3a,b) were mainly contributed to by the $2p_y$ and $2p_z$ orbitals of the carbon atoms, and neither PGNTs nor GPNTs had any contribution from the $2p_x$ orbitals around the band gap.

It is important to note that although hydrogen did not significantly contribute to the DOS, its small contribution did nevertheless result in an increase in the band gap energy for all models and chiralities analyzed; however, for PGNT and GPNT, the band gap energy difference was much higher than in the others and seemed to be more sensitive to the hydrogen contribution. The increases in the band gap energy for these models were around 3.05 eV (367%), and for PBNNT and IGP-BNNT, around 0.92 eV (∼16%). This large difference may be because of the chemical nature of the nanotubes consisting of only carbon (considered organic) compared to those that are considered inorganic and have a significant gap, as well as from effects arising from the structural differences in PG-based and IGP-based nanotube pores.

As evident in Figures 4 and 5, both chiralities of the PBNNTs and IGP-BNNTs were flat around the band gap, indicating that the electrons had low mobility in this region. For the carbon-based porous nanotubes, Figure S2 shows that the bands of both chiralities of PGNTs were also flat around the band gap. However, as shown in Figure S3, GPNTs exhibited nonflat bands around the band gap region, indicating good dispersion and higher electron mobility, as shown in the respective single-layer structure.

3.3. Elastic and Piezoelectric Properties. An understanding of the mechanical properties necessary to predict how the system will react when external forces are applied on the structure can lead to potential new applications.

As nanotubes have only one periodic dimension, therefore, there is only one elastic constant and one piezoelectric constant, namely, C_{11} and e_{11}, respectively. Both constants indicate how the nanotube responds to pressure and electrical response when stress is applied.

The elastic constant C_{11} is defined as the second derivative of the energy gradient with respect to the applied strain ε_1, divided by the equilibrium nanotube volume V, which can be approximated as the surface area of a one-atom thick cylinder with radius R and length L

$$C_{11} = \frac{1}{V}\frac{\partial^2 E}{\partial {\varepsilon_1}^2}\bigg|_0 \tag{1}$$

The single-layer elastic constants were calculated in the same way as in our previous work,[23] and the same methodology was applied to PBNNTs, IGP-BNNTs, PGNTs, and GPNTs.

The piezoelectric constant e_{11} is defined as the first derivative of the polarization (P) with respect to the strain (μ) over a constant electric field (ϵ), divided by the equilibrium volume V, which follows the same configuration as given above

$$e_{11} = \frac{1}{V}\frac{\partial P_1}{\partial \mu_{11}}\bigg|_\epsilon \tag{2}$$

The piezoelectric behavior can be separated into two types, the direct piezoelectricity which refers to a change in electric polarization when some materials are subjected to stresses, and the converse piezoelectricity which refers to a deformation caused by the application of an electric field.

To calculate the elastic constant C_{11}, three different diameters were chosen for each chirality, with n = 10, 20,

DOI: 10.1021/acsomega.8b01634
ACS Omega 2018, 3, 13413−13421

and 30, giving a total of 24 nanotubes analyzed to evaluate the trend. Table 1 summarizes the C_{11} for both chiralities of each nanotube. Because of the structural configuration, only zigzag nanotubes have a piezoelectric response.[44,45]

Table 1. Elastic Constant (C_{11}, GPa) of Armchair (n, n) and Zigzag (n, 0) Porous Nanotubes

	chirality	PBNNT	IGP-BNNT	PGNT	GPNT
C_{11}	(10, 10)	631.91	1082.56	762.86	1297.10
	(20, 20)	656.60	1084.27	760.15	1297.45
	(30, 30)	665.39	1083.81	760.88	1297.34
	(10, 0)	487.46	1077.88	590.66	1286.62
	(20, 0)	578.70	1080.76	627.51	1295.41
	(30, 0)	618.48	1083.16	640.33	1296.68

To compare the elastic properties with the literature, it is interesting to use the Young's modulus (Y) (often referred to as the stiffness), as described by Dresselhaus et al.,[42] it was calculated using $Y = C_{11}$ as a first approximation of Young's modulus because that a direct comparison can be difficult.

Analysis of the elastic constants showed that armchair and zigzag PBNNTs (IGP-BNNTs) had an average Young's modulus of ∼655 (1083) and ∼520 (1080) GPa, respectively. The PGNTs (GPNTs) had an average Young's modulus for armchair and zigzag conformations of ∼760 (1297) and ∼620 (1295) GPa, respectively. As a reference, single-layer PBN, IGP-BN, PG, and GP have a Young's modulus of ∼348, ∼563, ∼293, and ∼649 GPa, respectively.[23]

The results showed that the transition from the single-layer surface to nanotubes effectively doubled the stiffness of the structures along the nanotube axis direction. The armchair conformation of PGNTs showed a slightly higher tolerance to stress along the axis direction than did the zigzag conformation, although for GPNTs, both nanotube conformations showed approximately the same stiffness. The experimental value of the stiffness of typical single-walled carbon nanotubes is 1.25 TPa,[46] which is surprisingly close to the values obtained for the GPNTs, despite the latter having a higher porosity than CNTs, meanwhile if compared to our calculation for CNTs (∼2.04 TPa) it is ∼37% smaller. Nevertheless, this indicated that the structure was highly reinforced upon rolling, suggesting a possible application as a fiber composite reinforcement.

PBNNTs showed a very similar behavior to PGNTs in that the armchair conformation had a higher rigidity along the nanotube axis direction than did the zigzag conformation. IGP-BNNTs showed only a small variation in the stiffness for both armchair and zigzag conformations. Single-walled boron nitride nanotubes (SWBNNTs) have an average elastic modulus of ∼722 GPa, measured experimentally using the electric field-induced resonance method inside transmission electron microscopy,[47] which is higher than that calculated for PBNNTs and smaller than IGP-BNNTs; however, if compared with our calculations for BNNTs (∼1.65 GPa), the latter is ∼34% smaller. This indicated that both PBNNTs and IGP-BNNTs had a lower rigidity than SWBNNTs, as they are more deformable in the nanotube axis direction, but the IGP-BNNTs have the same behavior found for GPNTs as compared to nonporous nanotubes.

These results indicated that BN-based porous nanotubes were less susceptible to deformation along their axis direction compared to carbon-based nanotubes, as they have a slightly smaller stiffness; however, both nonhydrogenated porous nanotubes showed a significant increase in their stiffness compared to their respective single layers.

Additionally, PGNTs and PBNNTs showed a slight dependency of the elastic constant on the diameter in the zigzag conformation, whereas GPNTs and IGP-BNNTs did not show any such diameter dependence.

Also, it was observed that porous surfaces did not show any piezoelectric response, with the exception of PBN, which had very small piezoelectric constants of 5.46×10^{-5} C/m^2 (e_{11}) and −0.10 C/m^2 (e_{21}). The rolled-up surfaces maintained nonpiezoelectricity, with the exception of zigzag PBNNTs, whose piezoelectric constant does not have any diameter dependence, unlike the behavior observed for the elastic constants. The average value of the direct piezoelectric response was 0.44 C/m^2, 50% smaller than that for zigzag BNNTs (without pores) and showed a difference of only +0.10 C/m^2 compared to an hBN (0001) surface. Compared to other commonly used piezoelectric materials such as $BaTiO_3$[44] and ZnO,[45] the piezoelectricity of PBNNTs was ∼15.3 and ∼2.7 times smaller, respectively. The converse piezoelectric response was not observed.

One way to improve the piezoelectricity is to make structural deformations. For this purpose, strain was applied along the nanotube axis direction to simulate 5.0, 10.0, 15.0, 20.0, 25.0, and 30% expansion; the results are depicted in Table 2. Upon expansion, the piezoelectric constant increased by ∼7, ∼42, ∼222, ∼1321 and then starts to drop for ∼963 and 724%,

Table 2. Piezoelectric Constant and Topological Analysis of (3, 0) PBNNTs and (3, 0) IGP-BNNTs at the BCP: B(N)−BCP Distance (d_{BCP-B}, d_{BCP-N}, Å), Charge Density ($\rho(\mathbf{r})$), Laplacian of Electron Density ($\nabla^2\rho(\mathbf{r})$), $|V|/G$ Ratio, Bond Degree ($H/\rho(\mathbf{r})$), Ellipticity (ε), and Bond Type[a]

		piezoelectric constant and BCPs								
	strain (%)	e_{11}	E_{gap}	d_{BCP-B}	d_{BCP-N}	$\nabla^2\rho$	$\|V\|/G$	$H/\rho(\mathbf{r})$	ε	bond
PBNNT	0.0	0.43	6.35	0.49	0.99	0.142	1.837	−0.987	0.008	trans
	5.0	0.40	6.06	0.50	1.02	0.078	1.897	−0.981	0.010	trans
	10.0	0.61	5.92	0.52	1.06	−0.033	2.059	−0.972	0.012	cov
	15.0	1.39	5.92	0.57	1.13	−0.160	2.521	−0.934	0.017	cov
	20.0	6.12	5.93	0.81	1.24	−0.078	3.708	−0.450	0.013	cov
	25.0	4.58	3.30	1.28	1.58	0.004	1.617	−0.083	0.027	inter
	30.0	3.55	2.29	1.53	1.85	0.007	0.618	0.069	0.102	inter
IGP-BNNT	0.0	0.00	5.54	0.48	0.97	0.262	1.736	−0.969	0.028	trans

[a]The cov, trans, and inter notation refers to covalent, transition, and interaction bond type.

DOI: 10.1021/acsomega.8b01634
ACS Omega 2018, 3, 13413−13421

respectively; where from 15%, the same piezoelectric response than hBN was achieved.

Usually, the equilibrium structure of the zigzag nanotube has a natural piezoelectricity; in our particular case, the positive strain along its periodic direction leads to an increase on the polarizability and at the same time the improvement of the piezoelectricity. This increment can be assigned to two factors: first, the broken symmetry with the loss of its periodicity and second, the increase of the dipole momentum.

These results indicate that deformations can significantly alter the piezoelectric properties, making them a good candidate for electromechanical devices. Also, it was observed via topological analysis (Table 2) that when expansion reaches 20%, the nanotube almost reaches the limit of its elastic behavior, and the B−N bond starts to become a long-range interaction. When the strain is applied, it was observed that there was a change in B−N-type bond, the Laplacian value became negative, and the ratio $|V|/G > 2$, indicating that the bond changes from transitory (for zero strain applied) to covalent (above 5%). Despite the covalent bond, the BCP are closer to the boron atoms, ∼0.63 Å.

This analysis confirms that even with the increasing of 20% in the nanotube length, the B−N bond is almost preserved and the long-range interaction still maintains the nanotube structure. However, above 20% strain, the piezoelectric constant starts to drop and the bonding may break; this understanding can be induced by the vanishing of the electron density in the BCP, indicating a bond weakening. The representation of this behavior can be seen in Figure 6, as well as the Laplacian and bond degree behavior over a strain can be seen in Figures S4 and S5 (see Supporting Information).

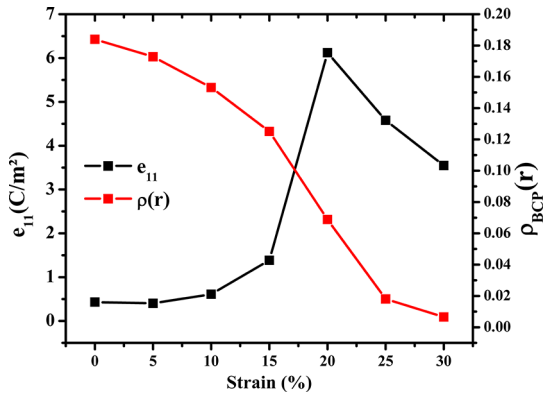

Figure 6. Uniaxial strain influence on the piezoelectric response and electron density at the BCP for (3, 0) PBNNT.

One way to achieve such a strain is using a nanofilm composed by aligned nanotubes deposited over a stretchable substrate and measuring the relative resistance of the system, as done for CNTs to use as a strain sensor for human body movement.[48]

4. CONCLUSIONS

The influence of the strain on the piezoelectric properties of PBNNTs have been studied by means of periodic method in a DFT/B3LYP(12%) framework. The positive strain (expansion) on the periodic direction of the nanotube reveals a significant increase in the piezoelectric response, showing up an effective means for controlling the piezoelectricity of the system. The piezoelectricity is increasing until 20% of strain, after this value, was possible to observe the limit of the expansion and the fracture of the structure. The elastic analysis showed that the porous armchair conformation has a higher stiffness than the zigzag nanotube. The calculated band gap energy is dependent of the diameter, with most of the structures converging to their respective single-layer structures. Moreover, for comparison purposes, the properties of porous carbon nanotubes were also simulated. In particular, the elastic properties of GPNTs showed similar values to nonporous carbon nanotubes, indicating that they are suitable for potential applications in the reinforcement of fiber composites.

The information raised here should be useful for experimentalists in the sense to direct their synthesis and analysis with respect to some specific necessity as well for theoretical scientists which could explore more properties and applications.

Until the present moment only the PG and GP surfaces were obtained experimentally; however, there is no synthesis evidence of both PGNTs and PBNNTs, but we hope they could be synthetized in the near future.

5. COMPUTATIONAL DETAILS

Computational simulations were performed using a periodic DFT method, implemented in CRYSTAL17[49] software. As the choice of an appropriate functional that accurately describes the structural and electronic properties are important, based on previous work on PG and PBN single-layer structures,[23] we used a modified B3LYP (12% hybrid) functional, in which the hybrid percentage was described as a fraction of mixing of exact Hartree−Fock (HF) and DFT exchange contributions in the modified functional. The following equation describes the modified B3LYP functional: $E_{xc} = (1 - A)\cdot(E_x^{LDA} + 0.9\cdot E_x^{BECKE}) + A\cdot E_x^{HF} + 0.19\cdot E_c^{LDA} + 0.81\cdot E_c^{GGA}$, where A is the hybrid percentage ($A = 0.12$). The carbon, boron, nitrogen, and hydrogen atoms were described by a TZVP basis set.[41]

All stationary points were characterized as minima by diagonalizing the Hessian matrix with respect to the unit cell parameters and atomic coordinates. The convergence was checked on the gradient components and nuclear displacements, with tolerances on their root-mean-squares set to 0.0001 and 0.0004 a.u., respectively.

The level of accuracy in evaluating the infinite Coulomb and HF exchange series was controlled by five α_i parameters, with $i = 1-5$, such that two-electron contributions were neglected when the overlap between atomic functions was below $10^{-\alpha_i}$. The five α_i parameters were set to 10, 10, 10, 20, and 40, and the shrinking factor for the Pack−Monkhorst and Gilat nets was set to 20.

The DOS and band structure were analyzed using the same k-point sampling employed for diagonalization of the Fock matrix in the optimization process.

The electron density was further analyzed by quantum theory of atoms in molecules and crystals (QTAIMAC), carried out via TOPOND program[50] incorporated in CRYSTAL17, which is a theory that provides a quantum description of the probability of electron density location, therefore, offering important information on the chemical bonds, cages, rings, and nuclei, which leads to fundamental understanding of the type interaction between the atoms and the modifications induced by structural modifications.

The topological properties were evaluated by analyzing the critical point of the bonds, which are called BCPs. A critical

DOI: 10.1021/acsomega.8b01634
ACS Omega 2018, 3, 13413−13421

point (CP) in the electron density, $\rho(\mathbf{r})$, is a point where the gradient of the density vanishes ($\nabla\rho(\mathbf{r}) = 0$). Each CP can be classified in terms of the eigenvalues, λ_1, λ_2, and λ_3 of the Hessian matrix; consequently, each CP can be labeled with two indices (r, s) where r is the number of nonzero eigenvalues values and s is the sum of the algebraic signs of the eigenvalues. Therefore, in a particular case of the BCP, (r, s) corresponds to (3, −1) and indicates a saddle point in the electron density scalar field, with a local minimum along the interatomic direction and two maxima in perpendicular directions.

Several quantities can be evaluated at BCP to define the bond character, such as electron density, Laplacian ($\nabla^2\rho(\mathbf{r})$), ratio of potential energy density, and kinetic energy density ($V(\mathbf{r})/G(\mathbf{r})$), and the total electronic energy density ($H = V(\mathbf{r}) + G(\mathbf{r})$) which defines the bond degree $H/\rho(\mathbf{r})$. These values can indicate ionic (as hydrogen bond or van der Waals interactions), covalent, or transitory bond.

Besides that, the bond shape is described by the ellipticity parameter (ε), which indicates how and in which direction the density is mostly polarized. An ε value close to zero indicates a localized density (which presents a cylindrical shape), characteristic of an ionic bond or covalent bond in a polar molecule. On the other hand, ε = ∼1 indicates an elliptical bond shape with a more "scattered" density between the two attractors.

■ ASSOCIATED CONTENT

Supporting Information

The Supporting Information is available free of charge on the ACS Publications website at DOI: 10.1021/acsomega.8b01634.

Side view of porous nanotubes with the inter-ring and intra-ring highlighted; brief commentary of the porous nanotubes structural properties and structural data presentation; band structure and DOS of the (10, 10) and (10, 0) PGNT and GPNT; and uniaxial strain influence on the piezoelectric response and on the topological properties (PDF)

■ AUTHOR INFORMATION

Corresponding Author

*E-mail: jr.sambrano@unesp.br.

ORCID

Elson Longo: 0000-0001-8062-7791

Julio R. Sambrano: 0000-0002-5217-7145

Notes

The authors declare no competing financial interest.

■ ACKNOWLEDGMENTS

This work was supported by the Brazilian funding agencies, CAPES (grant nos. 787027/2013 and 8881.068492/2014-01) and FAPESP (grant nos. 2013/07296-2, 2016/07476-9, and 2016/25500-4). The computational facilities were supported by resources supplied by the Molecular Simulations Laboratory, São Paulo State University, Bauru, Brazil.

■ REFERENCES

(1) Geim, A. K.; Novoselov, K. S. The Rise of Graphene. *Nat. Mater.* **2007**, *6*, 183−191.

(2) Elias, D. C.; Nair, R. R.; Mohiuddin, T. M. G.; Morozov, S. V.; Blake, P.; Halsall, M. P.; Ferrari, A. C.; Boukhvalov, D. W.; Katsnelson, M. I.; Geim, A. K.; et al. Control of Graphene's Properties by Reversible Hydrogenation: Evidence for Graphane. *Science* **2009**, *323*, 610−613.

(3) Xu, Y.; Shi, G.; Duan, X. Self-Assembled Three-Dimensional Graphene Macrostructures: Synthesis and Applications in Supercapacitors. *Acc. Chem. Res.* **2015**, *48*, 1666−1675.

(4) Chen, Y.; Tan, C.; Zhang, H.; Wang, L. Two-Dimensional Graphene Analogues for Biomedical Applications. *Chem. Soc. Rev.* **2015**, *44*, 2681−2701.

(5) Fadel, T. R.; Fahmy, T. M. Immunotherapy Applications of Carbon Nanotubes: From Design to Safe Applications. *Trends Biotechnol.* **2014**, *32*, 198−209.

(6) Wang, Q.; Wang, X.; Chai, Z.; Hu, W. Low-Temperature Plasma Synthesis of Carbon Nanotubes and Graphene Based Materials and Their Fuel Cell Applications. *Chem. Soc. Rev.* **2013**, *42*, 8821−8834.

(7) Quhe, R.; Ma, J.; Zeng, Z.; Tang, K.; Zheng, J.; Wang, Y.; Ni, Z.; Wang, L.; Gao, Z.; Shi, J.; et al. Tunable Band Gap in Few-Layer Graphene by Surface Adsorption. *Sci. Rep.* **2013**, *3*, 1794.

(8) Paupitz, R.; Autreto, P. A. S.; Legoas, S. B.; Srinivasan, S. G.; van Duin, A. C. T.; Galvão, D. S. Graphene to Fluorographene and Fluorographane: A Theoretical Study. *Nanotechnology* **2013**, *24*, 035706.

(9) Stankovich, S.; Dikin, D. A.; Piner, R. D.; Kohlhaas, K. A.; Kleinhammes, A.; Jia, Y.; Wu, Y.; Nguyen, S. B. T.; Ruoff, R. S. Synthesis of Graphene-Based Nanosheets via Chemical Reduction of Exfoliated Graphite Oxide. *Carbon N. Y.* **2007**, *45*, 1558−1565.

(10) Flores, M. Z. S.; Autreto, P. A. S.; Legoas, S. B.; Galvao, D. S. Graphene to Graphane: A Theoretical Study. *Nanotechnology* **2009**, *20*, 465704.

(11) Ni, Z. H.; Yu, T.; Lu, Y. H.; Wang, Y. Y.; Feng, Y. P.; Shen, Z. X. Uniaxial Strain on Graphene: Raman Spectroscopy Study and Band-Gap Opening. *ACS Nano* **2008**, *2*, 2301−2305.

(12) Banhart, F.; Kotakoski, J.; Krasheninnikov, A. V. Structural Defects in Graphene. *ACS Nano* **2011**, *5*, 26−41.

(13) Giovannetti, G.; Khomyakov, P. A.; Brocks, G.; Karpan, V. M.; Van Den Brink, J.; Kelly, P. J. Doping Graphene with Metal Contacts. *Phys. Rev. Lett.* **2008**, *101*, 4−7.

(14) Lukose, V.; Shankar, R.; Baskaran, G. Novel Electric Field Effects on Landau Levels in Graphene. *Phys. Rev. Lett.* **2007**, *98*, 116802.

(15) Lalmi, B.; Oughaddou, H.; Enriquez, H.; Kara, A.; Vizzini, S.; Ealet, B.; Aufray, B. Epitaxial Growth of a Silicene Sheet. *Appl. Phys. Lett.* **2010**, *97*, 223109.

(16) Aufray, B.; Kara, A.; Vizzini, S.; Oughaddou, H.; Léandri, C.; Ealet, B.; Le Lay, G. Graphene-like Silicon Nanoribbons on Ag(110): A Possible Formation of Silicene. *Appl. Phys. Lett.* **2010**, *96*, 183102.

(17) Dávila, M. E.; Xian, L.; Cahangirov, S.; Rubio, A.; Le Lay, G. Germanene: A Novel Two-Dimensional Germanium Allotrope Akin to Graphene and Silicene. *New J. Phys.* **2014**, *16*, 095002.

(18) Golberg, D.; Bando, Y.; Huang, Y.; Terao, T.; Mitome, M.; Tang, C.; Zhi, C. Boron Nitride Nanotubes and Nanosheets. *ACS Nano* **2010**, *4*, 2979−2993.

(19) Bieri, M.; Treier, M.; Cai, J.; Aït-Mansour, K.; Ruffieux, P.; Gröning, O.; Gröning, P.; Kastler, M.; Rieger, R.; Feng, X.; et al. Porous Graphenes: Two-Dimensional Polymer Synthesis with Atomic Precision. *Chem. Commun.* **2009**, 6919.

(20) Li, Y.; Zhou, Z.; Shen, P.; Chen, Z. Two-Dimensional Polyphenylene: Experimentally Available Porous Graphene as a Hydrogen Purification Membrane. *Chem. Commun.* **2010**, *46*, 3672.

(21) Du, A.; Zhu, Z.; Smith, S. C. Multifunctional Porous Graphene for Nanoelectronics and Hydrogen Storage: New Properties Revealed by First Principle Calculations. *J. Am. Chem. Soc.* **2010**, *132*, 2876−2877.

(22) Ding, Y.; Wang, Y.; Shi, S.; Tang, W. Electronic Structures of Porous Graphene, BN, and BC2N Sheets with One- and Two-Hydrogen Passivations from First Principles. *J. Phys. Chem. C* **2011**, *115*, 5334−5343.

(23) Fabris, G. S. L.; Marana, N. L.; Longo, E.; Sambrano, J. R. Theoretical Study of Porous Surfaces Derived from Graphene and Boron Nitride. *J. Solid State Chem.* **2017**, *258*, 247.

DOI: 10.1021/acsomega.8b01634
ACS Omega 2018, 3, 13413−13421

(24) Brunetto, G.; Autreto, P. A. S.; Machado, L. D.; Santos, B. I.; dos Santos, R. P. B.; Galvão, D. S. Nonzero Gap Two-Dimensional Carbon Allotrope from Porous Graphene. *J. Phys. Chem. C* **2012**, *116*, 12810−12813.
(25) Totani, R.; Grazioli, C.; Zhang, T.; Bidermane, I.; Lüder, J.; de Simone, M.; Coreno, M.; Brena, B.; Lozzi, L.; Puglia, C. Electronic Structure Investigation of Biphenylene Films. *J. Chem. Phys.* **2017**, *146*, 054705.
(26) Du, Q.-S.; Tang, P.-D.; Huang, H.-L.; Du, F.-L.; Huang, K.; Xie, N.-Z.; Long, S.-Y.; Li, Y.-M.; Qiu, J.-S.; Huang, R.-B. A New Type of Two-Dimensional Carbon Crystal Prepared from 1,3,5-Trihydroxybenzene. *Sci. Rep.* **2017**, *7*, 40796.
(27) Yu, Y.-X. Graphenylene: a promising anode material for lithium-ion batteries with high mobility and storage. *J. Mater. Chem. A* **2013**, *1*, 13559.
(28) Song, Q.; Wang, B.; Deng, K.; Feng, X.; Wagner, M.; Gale, J. D.; Müllen, K.; Zhi, L. Graphenylene, a Unique Two-Dimensional Carbon Network with Nondelocalized Cyclohexatriene Units. *J. Mater. Chem. C* **2013**, *1*, 38−41.
(29) Woods, C. R.; Britnell, L.; Eckmann, A.; Ma, R. S.; Lu, J. C.; Guo, H. M.; Lin, X.; Yu, G. L.; Cao, Y.; Gorbachev, R. V.; et al. Commensurate−incommensurate Transition in Graphene on Hexagonal Boron Nitride. *Nat. Phys.* **2014**, *10*, 451−456.
(30) Cassabois, G.; Valvin, P.; Gil, B. Hexagonal Boron Nitride Is an Indirect Bandgap Semiconductor. *Nat. Photonics* **2016**, *10*, 262−266.
(31) Hankel, M.; Searles, D. J. Lithium Storage on Carbon Nitride, Graphenylene and Inorganic Graphenylene. *Phys. Chem. Chem. Phys.* **2016**, *18*, 14205−14215.
(32) Baughman, R. H. Carbon Nanotubes–the Route Toward Applications. *Science* **2002**, *297*, 787−792.
(33) Lu, H.; Zheng, F.; Guo, M.; Zhang, M. One-Step Electrodeposition of Single-Crystal ZnO Nanotube Arrays and Their Optical Properties. *J. Alloys Compd.* **2014**, *588*, 217−221.
(34) Freitas, R. G.; Santanna, M. A.; Pereira, E. C. Dependence of TiO2 Nanotube Microstructural and Electronic Properties on Water Splitting. *J. Power Sources* **2014**, *251*, 178−186.
(35) Jiao, Y.; Du, A.; Zhu, Z.; Rudolph, V.; Smith, S. C. A Density Functional Theory Study of CO2 and N2 Adsorption on Aluminium Nitride Single Walled Nanotubes. *J. Mater. Chem.* **2010**, *20*, 10426.
(36) Ozgit-Akgun, C.; Kayaci, F.; Donmez, I.; Uyar, T.; Biyikli, N. Template-Based Synthesis of Aluminum Nitride Hollow Nanofibers Via Plasma-Enhanced Atomic Layer Deposition. *J. Am. Ceram. Soc.* **2013**, *96*, 916−922.
(37) Chigo Anota, E.; Cocoletzi, G. Influence of Point Defects on the Structural and Electronic Properties of SiC Nanotubes. *Open Chem.* **2014**, *12*, 53−59.
(38) Duan, Y.; Zhang, J.; Xu, K. Structural and Electronic Properties of Chiral Single-Wall Copper Nanotubes. *Sci. China Physics, Mech. Astron.* **2014**, *57*, 644−651.
(39) Koch, A. T.; Khoshaman, A. H.; Fan, H. D. E.; Sawatzky, G. A.; Nojeh, A. Graphenylene Nanotubes. *J. Phys. Chem. Lett.* **2015**, *6*, 3982−3987.
(40) Fabris, G. S. L.; Junkermeier, C. E.; Paupitz, R. Porous Graphene and Graphenylene Nanotubes: Electronic Structure and Strain Effects. *Comput. Mater. Sci.* **2017**, *140*, 344−355.
(41) Peintinger, M. F.; Oliveira, D. V.; Bredow, T. Consistent Gaussian Basis Sets of Triple-Zeta Valence with Polarization Quality for Solid-State Calculations. *J. Comput. Chem.* **2013**, *34*, 451−459.
(42) Dresselhaus, M. S.; Dresselhaus, G.; Saito, R. Physics of Carbon Nanotubes. *Carbon* **1995**, *33*, 883−891.
(43) Wilder, J. W. G.; Venema, L. C.; Rinzler, A. G.; Smalley, R. E.; Dekker, C. Electronic Structure of Atomically Resolved Carbon Nanotubes. *Nature* **1998**, *391*, 59−62.
(44) Zhang, J.; Wang, C.; Bowen, C. Piezoelectric Effects and Electromechanical Theories at the Nanoscale. *Nanoscale* **2014**, *6*, 13314−13327.
(45) Marana, N. L.; Casassa, S. M.; Sambrano, J. R. Piezoelectric, Elastic, Infrared and Raman Behavior of ZnO Wurtzite under Pressure from Periodic DFT Calculations. *Chem. Phys.* **2017**, *485*−*486*, 98−107.
(46) Treacy, M. M. J.; Ebbesen, T. W.; Gibson, J. M. Exceptionally High Young's Modulus Observed for Individual Carbon Nanotubes. *Nature* **1996**, *381*, 678−680.
(47) Suryavanshi, A. P.; Yu, M.-F.; Wen, J.; Tang, C.; Bando, Y. Elastic Modulus and Resonance Behavior of Boron Nitride Nanotubes. *Appl. Phys. Lett.* **2004**, *84*, 2527−2529.
(48) Yamada, T.; Hayamizu, Y.; Yamamoto, Y.; Yomogida, Y.; Izadi-Najafabadi, A.; Futaba, D. N.; Hata, K. A Stretchable Carbon Nanotube Strain Sensor for Human-Motion Detection. *Nat. Nanotechnol.* **2011**, *6*, 296−301.
(49) Dovesi, R.; Erba, A.; Orlando, R.; Zicovich-Wilson, C. M.; Civalleri, B.; Maschio, L.; Rérat, M.; Casassa, S.; Baima, J.; Salustro, S.; et al. Quantum-Mechanical Condensed Matter Simulations with CRYSTAL. *Wiley Interdiscip. Rev. Comput. Mol. Sci.* **2018**, *8*, No. e1360.
(50) Gatti, C.; Casassa, S. *TOPOND User's Manual*; CNR-CSRSRC: Milano, 2013.

DOI: 10.1021/acsomega.8b01634
ACS Omega 2018, 3, 13413−13421